

# Synthesis, characterization, and catalytic application of Au/ZnO nanocomposites prepared by coprecipitation

B. Donkova · P. Vasileva · D. Nihtianova ·  
N. Velichkova · P. Stefanov · D. Mehandjiev

Received: 20 December 2010 / Accepted: 22 March 2011 / Published online: 7 April 2011  
© Springer Science+Business Media, LLC 2011

**Abstract** In this study, Au/ZnO nanocomposites of different gold contents (0.8, 2.5, and 9%) and specific surface areas (from 41 to 51 m<sup>2</sup>/g) were synthesized via a coprecipitation method. The pure ZnO was obtained at the same experimental conditions. The samples were characterized by XRD, SEM, TEM, HRTEM, and XPS. The influence of gold nanoparticles (Au-NPs) loading on the catalytic activity of Au/ZnO nanocomposite was studied in the model reaction of CO oxidation. Spherical shape and homogeneous distribution of Au-NPs were observed in all samples prepared. The average size of Au-NPs in the obtained catalysts are almost the same (about 4 nm) allowing the studied effect to be manifested. The decrease of intrinsic catalytic activity of the coprecipitated Au/ZnO nanocomposites follows the sequence 2.5, 9, and 0.8% Au, as corresponding to the decrease of relative surface content of Au-NPs. It could be suggested that the catalytic activity

is noticeably influenced by the distribution of Au-NPs between the bulk and surface of catalysts.

## Introduction

In the middle of the 1980s, Mastake Haruta et al. [1, 2] and Graham Hutchings [3] reported for the first time of the high catalytic activity of the gold and their works were the turning point in the investigations and application of gold as a catalyst. This breakthrough provoked astonishing escalation of the scientific interest in the nano-gold heterogeneous and homogeneous catalysis, and today it is one of the fastest developing subjects in material science [4]. The results obtained have been summarized and analyzed in a number of reviews and books [5–10].

Nanometer-sized gold particles (Au-NPs) supported on oxides or carbides are extremely active in several reactions, e.g., the partial oxidation of hydrocarbons, the water–gas shift reaction, and the reduction of nitrogen oxides. However, their best performance is in the reaction of CO oxidation, where they exceed the activity of catalysts based upon the platinum group metals at temperatures below 400 K [11, 12]. CO oxidation is an important subject in a large number of industrial and environmental protection processes. On the other hand, it is a simple model reaction for testing the catalytic activity and revealing the relation between activity and preparation methods, composition, and structure of the oxide-supported gold catalysts.

In reactions of complete oxidation ZnO has been less studied as a support in comparison with other oxides, as Fe<sub>2</sub>O<sub>3</sub>, Al<sub>2</sub>O<sub>3</sub>, NiO, and TiO<sub>2</sub>, due to its own lower activity, but growing interest toward ZnO in the latest years was observed. So far, there are studies in the literature on the catalytic activity of ZnO-supported gold nanoparticles

B. Donkova (✉) · P. Vasileva (✉)  
Faculty of Chemistry, University of Sofia, 1 J. Bourchier Ave,  
1164 Sofia, Bulgaria  
e-mail: bdonkova@inorg.chem.uni-sofia.bg

P. Vasileva  
e-mail: pvasileva@chem.uni-sofia.bg

D. Nihtianova  
Institute of Mineralogy and Crystallography, Bulgarian  
Academy of Sciences, Acad. G. Bonchev Str., bl. 107,  
1113 Sofia, Bulgaria

D. Nihtianova · N. Velichkova · P. Stefanov  
Institute of General and Inorganic Chemistry, Bulgarian  
Academy of Sciences, Acad. G. Bonchev Str., bl. 11, 1113 Sofia,  
Bulgaria

D. Mehandjiev  
Institute of Catalysis, Bulgarian Academy of Sciences, Acad.  
G. Bonchev Str., bl. 11, Sofia 1113, Bulgaria

(Au-NPs) mainly in the reaction of CO oxidation [5, 13–18], but also in PROX [19–21], WGS [22], and some other reactions. Au/ZnO nanocomposites are also a promising system for application as a photocatalyst [23] and sensor for ethanol [24–26], CO [27–29], and VOCs [30].

Oxide-supported gold catalysts are traditionally prepared using aqueous solution synthesis methods. The most quoted ones are coprecipitation and deposition–precipitation, which produce highly dispersed Au-NPs and more active catalysts for CO oxidation, as compared to the impregnation and photo-deposition [6, 7]. For the first time small gold particles supported on various oxides, such as  $\text{Fe}_2\text{O}_3$ ,  $\text{NiO}$ , and  $\text{Co}_3\text{O}_4$ , were synthesized by Haruta et al. applying a coprecipitation method [2, 31]. These catalysts were prepared by adding sodium carbonate to aqueous solution of  $\text{HAuCl}_4$  and the corresponding metal nitrate. This relatively simple procedure has not been changed up to the present and is also applied for the preparation of Au-NPs supported on ZnO [5, 15–18, 32].

The dependence of the catalytic activity on the type of precipitating agent, calcination temperature, acidity and temperature of the synthesis procedure, and precipitate aging were investigated in Ref. [17, 18]. It was established that (i)  $\text{Na}_2\text{CO}_3$  is a better precipitant than  $(\text{NH}_4)_2\text{CO}_3$ ,  $\text{NaOH}$ , and  $\text{NH}_4\text{OH}$  [17]; (ii) temperature of 80 °C and aging time of 1 h lead to a better catalytic performance of Au/ZnO [18]. These optimal reaction conditions were adopted and applied in this study for the preparation of Au/ZnO nanocomposite. The size effect of ZnO-supported Au-NPs on the catalyst performance has been already reported: the smaller the particle size, the higher the catalytic activity is [14]. To the best of our knowledge, there are no literature data concerned with the effect of gold loading on the activity of coprecipitated Au/ZnO catalysts in the process of CO oxidation. The aim of this study is the synthesis of coprecipitated Au/ZnO nanocomposites with different gold loadings, their structural characterization, and assessment of the influence of Au-NPs loading on the catalytic activity in the model reaction of CO oxidation. The Au-NPs in all obtained so catalysts are of almost the same size (about 4 nm), thus allowing the studied effect to be manifested.

## Experimental

### Catalyst preparation

Three starting solutions of  $\text{HAuCl}_4$  with target molar concentrations of 0.01, 0.02, and 0.09 mol/dm<sup>3</sup> were prepared using  $\text{HAuCl}_4 \cdot 3\text{H}_2\text{O}$  (Panreac, Spain). The relevant experimental values determined by atomic absorption spectroscopy (AAS) were 0.007, 0.022, and 0.087 mol/dm<sup>3</sup>, respectively. The analytical determination of the real

gold concentrations is necessary because of the substantial inaccuracy in the concentration of the prepared solutions that could be allowed, due to the dissolution of the gold precursor in its own crystalline water.

A series of ZnO-supported Au catalysts with desired metal loading were prepared by coprecipitation under the experimental conditions recommended in Ref. [18]. In brief, 100 mL of 0.1 M  $\text{Zn}(\text{NO}_3)_2$  solution, heated to 80 °C, was mixed with 5 mL of  $\text{HAuCl}_4$  starting solution under continuous stirring.  $\text{Na}_2\text{CO}_3$  solution (0.25 M) was then added dropwise until pH 8.5 was reached. The precipitate was aged for 1 h at synthesis conditions, after that it was recovered by membrane filtration (Millipore membrane filter 8 µm) and washed several times with cold and hot water until no  $\text{Cl}^-$  ions were detected by  $\text{AgNO}_3$ . The product was dried initially in air, subsequently in oven at 90 °C for 16 h. Finally, the sample was calcined at 400 °C for 3 h. The nanocomposites obtained in this way are denoted, respectively, as 0.8-Au/ZnO, 2.5-Au/ZnO, and 9-Au/ZnO, where the numbers indicate the gold content in weight percentage. For comparison the pure ZnO was synthesized using the same procedure and experimental conditions.

### Catalyst characterization

Atomic absorbance spectroscopy was used to determine the actual amount of gold deposited on the ZnO support. The Au/ZnO powder was dissolved in aqua regia, followed by evaporation of the acid and dilution to the definite volume.

The X-ray diffraction (XRD) analysis was carried out on a Siemens powder diffractometer model D500 using  $\text{CuK}\alpha$  radiation in a  $2\theta$  diffraction interval of 25° to 85°. The refinement with Powder Cell software was used to identify the crystallographic phases present and to calculate the crystal lattice parameters and crystallite sizes (by Scherrer equation) from the XRD patterns. Diffraction data were processed using the Powder Cell program [33].

The specific surface area of the sample was determined by nitrogen adsorption at the boiling temperature of liquid nitrogen (77.4 K) using a conventional volume-measuring apparatus.

The morphological characterization was carried out by scanning electron microscope (SEM) observation using a JEOL JSM-5510 apparatus. The TEM investigations were performed by TEM JEOL 2100 with an accelerating voltage of 200 kV. The specimens were prepared by dispersing the nanocomposite powder in ethanol under ultrasonic treatment for 6 min. The suspensions were dripped on standard carbon/Cu grids. The histograms of Au-NP size distribution and average diameters were determined from different TEM images for each sample by measuring about 150 individual Au-NPs. The Image J software was used.

The X-ray photoelectron spectroscopy (XPS) studies were performed in a VG Escalab II electron spectrometer using AlK $\alpha$  radiation with energy of 1486.6 eV. The residual gas pressure in the analysis chamber was  $10^{-7}$  Pa. The line of C 1s at 284.6 eV was used as an internal standard for calibrating the binding energies ( $\text{BE} \pm 0.2$  eV).

#### Catalytic tests

The catalytic activity of the samples was studied in an isothermal plug flow reactor enabling operation under steady-state conditions without temperature gradients. The size of the catalyst particles (0.3–0.6 mm) was chosen taking into account the reactor diameter (6.0 mm) and the hourly space velocity (20,000/h) to reduce the effect of the pore diffusion. The gas feed flow rate was 4.4 l/h, the catalyst bed volume was 0.2 cm<sup>3</sup>, and the mass of the charged catalyst was 0.15–0.25 g. The catalytic oxidation of CO was performed at the temperature interval 130–320 °C, the oxidizing agent used being oxygen from synthetic air (a gas mixture: 21 vol.% O<sub>2</sub>; 79 vol.% N<sub>2</sub>). The preliminary treatment of the catalyst included heating in dry air flow at 120 °C for 1 h to remove moisture and adsorbed impurities. The CO flow was fed into the reactor by an Ismatec M62/6 pump (Switzerland).

The initial concentration of carbon monoxide was 0.5 vol.%. The carrier gas was synthetic air. A Maihak (O<sub>2</sub>/CO/CO<sub>2</sub>) gas analyzer was used to measure the CO and CO<sub>2</sub> concentrations with an accuracy of  $\pm 0.1$  ppm, while the oxygen measurement accuracy was  $\pm 100$  ppm.

## Results and discussion

### Nanocomposite characterization

The values of the specific surface area, nominal, and the actual gold loading of the obtained samples are presented in Table 1. The nominal loading of gold is calculated from the data of AAS analysis of the initial HAuCl<sub>4</sub> solutions, while the real loading is determined after dissolving the calcined samples in aqua regia. The efficiency of gold loading, calculated as a ratio of the real to nominal values, is also shown in Table 1.

The specific surface area of catalysts varies in the range of 41–51 m<sup>2</sup>/g and is comparable to the values obtained by other authors [15, 17]. It is important to note that the gold content in the initial reaction mixture does not have an effect on the efficiency of gold loading in the ZnO matrix at the studied experimental conditions. An efficiency of gold loading in the range of 86–93% is achieved for all nanocomposites prepared. These values are significantly

**Table 1** Specific surface area ( $A_{\text{BET}}$ ), nominal gold content, real gold content in weight percentage (Wt, %), and gold loading efficiency (%) of the samples studied

Sample	$A$ , m <sup>2</sup> /g	Au <sub>nominal</sub> , %	Au <sub>real</sub> , %	Loading efficiency, %
ZnO	46	—	—	—
0.8-Au/ZnO	46	0.85	0.78	91.8
2.5-Au/ZnO	51	2.66	2.49	93.6
9-Au/ZnO	41	10.52	9.06	86.1

higher than the 37.1%, calculated from the data in Ref. [18] for Au/ZnO obtained at similar experimental conditions without aging. Moreover, the reported decrease of gold content in Ref. [18] (from 2.6 to 1%) after the precipitate aging before the filtration step is not observed in our study.

The X-ray diffraction analysis was carried out for all synthesized samples, but only diffractograms for pure ZnO and Au/ZnO with highest gold loading are shown in Fig. 1. The refinement with Powder Cell software shows the presence of hexagonal phase (wurzite structure) of ZnO (JCPDS 36-1451) in all studied samples. The diffraction peaks of cubic gold in the studied range should be sought at  $2\theta$  of 38.217°, 44.431°, 64.636°, 77.624°, and 81.804° (JCPDS 04-0784) corresponding to the crystal planes (111), (200), (220), (311), and (222). These reflections are detected only in the diffractogram of the 9-Au/ZnO sample—that with the highest gold loading. Broad peaks are observed, due to the high dispersion of gold and the small particle size. As a result, most of them are overlapped by ZnO diffraction peaks. As expected, the gold peaks were not observed in the XRD patterns of other Au/ZnO nanocomposites, due to the low content of gold.

The ZnO crystal lattice parameters and average crystallite sizes derived from the XRD data are listed in Table 2, together with those of a standard (JCPDS 36-1451). The obtained values show that there is no substitution of zinc by gold atoms in the oxide crystal lattice. Despite of the different gold loadings in the Au/ZnO nanocomposites studied, the incorporation of Au-NPs in the ZnO matrix does not influence the crystal lattice parameters and the average crystallite size of the matrix. The crystallite size of Au-NPs was not determined from XRD data because the reliable estimation of gold crystallites requires higher peak intensities.

The SEM images depicted in Fig. 2 show that crystals of pure ZnO represent “rose-like” agglomerates with irregular arrangement of their rounded nanosized “leaflets” (<100 nm in thickness). The same morphology is observed for Au/ZnO nanocomposites even for the sample with the highest gold loading of 9%.

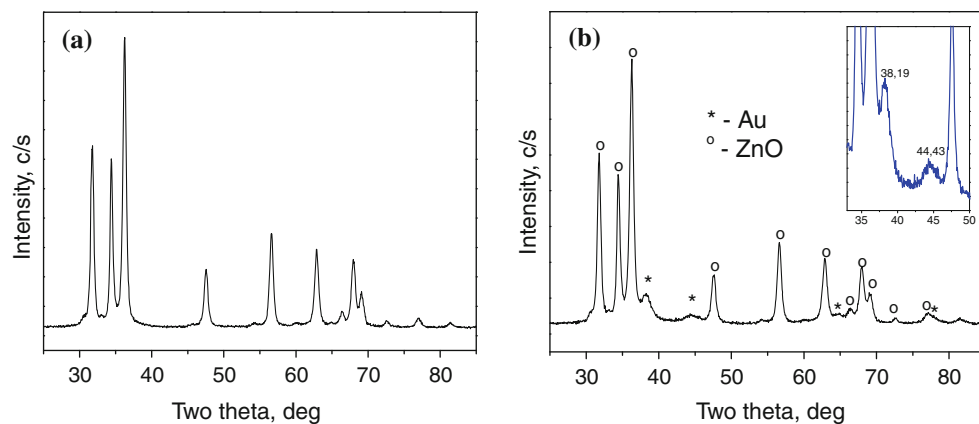
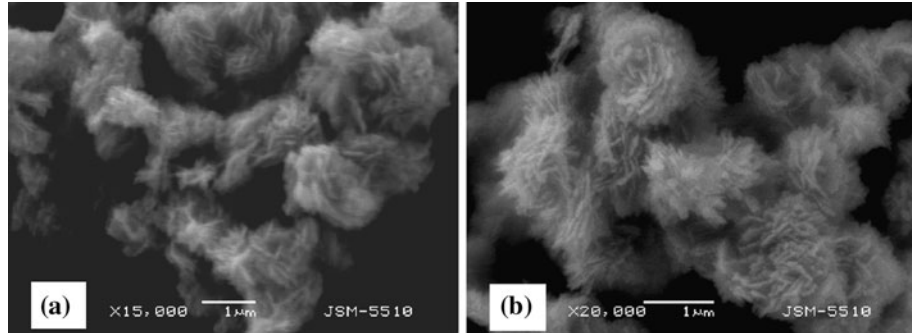


**Fig. 1** X-ray diffraction patterns of pure ZnO (a) and 9-Au/ZnO (b) (inset: the region of  $2\theta$  with the most intensive diffraction peaks of gold nanoparticles)

**Table 2** ZnO crystal lattice parameters, average crystallite sizes of ZnO, and average Au-NPs diameter of samples studied

Sample	Lattice parameters, Å SG P6 <sub>3</sub> mc		$d_{\text{cryst. ZnO}}$ , nm from XRD	$d_{\text{mean. Au}}$ , nm from TEM
	$a \pm 0.0002$	$c \pm 0.0002$		
Ref. 36-1451	3.2509	5.2071		—
ZnO	3.2505	5.2067	15	—
0.8-Au/ZnO	3.2514	5.2086	13	4.0 ± 1.1
2.5-Au/ZnO	3.2508	5.2078	16	4.1 ± 1.2
9-Au/ZnO	3.2520	5.2088	15	3.7 ± 0.7

**Fig. 2** SEM images of pure ZnO (a) and 9-Au/ZnO (b) samples



Bright field micrographs of Au/ZnO samples are presented in Fig. 3a–c. Small uniform Au-NPs (black dots) with prevailing spherical shape and homogeneous distribution in the ZnO matrix are observed. All the synthesized samples show a narrow size distribution of Au-NPs (Fig. 3d–f) with almost the same average particle diameter of ca. 4 nm (Table 2) that is typical for Au-NPs in coprecipitated Au/ZnO catalysts [15–17]. Moreover, our results show that the size of the deposited Au-NPs is not affected by the different gold loadings in Au/ZnO nanocomposites, as varying from 0.8 to 9% Au.

Experimental HRTEM image of 0.8-Au/ZnO sample is shown in Fig. 4, and the lattice spacing of 0.325 nm corresponding to hexagonal ZnO is measured and labeled on the

Fourier filtered image. The higher values of lattice spacing, measured in areas AI and AII (labeled on HRTEM), could be attributed to several of the basic zinc carbonates. This result is an evidence of some insignificant amount of ZnO precursor, present in Au/ZnO nanocomposites, calcined at temperature of 400 °C. According to the literature data, based on DTA, TG, and XRD analyses, the basic zinc carbonate ( $\text{Zn}_5(\text{CO}_3)_2(\text{OH})_6$  or  $\text{Zn}_4(\text{CO}_3)(\text{OH})_6 \cdot \text{H}_2\text{O}$ ) disappears at temperatures above 240 °C [17, 34]. However, the higher sensitivity of HRTEM analysis allowed us to identify traces of basic zinc carbonates in Au/ZnO composites, which could not be detected by XRD.

Selected area electron diffraction (SAED) patterns of samples with the lowest and the highest gold contents

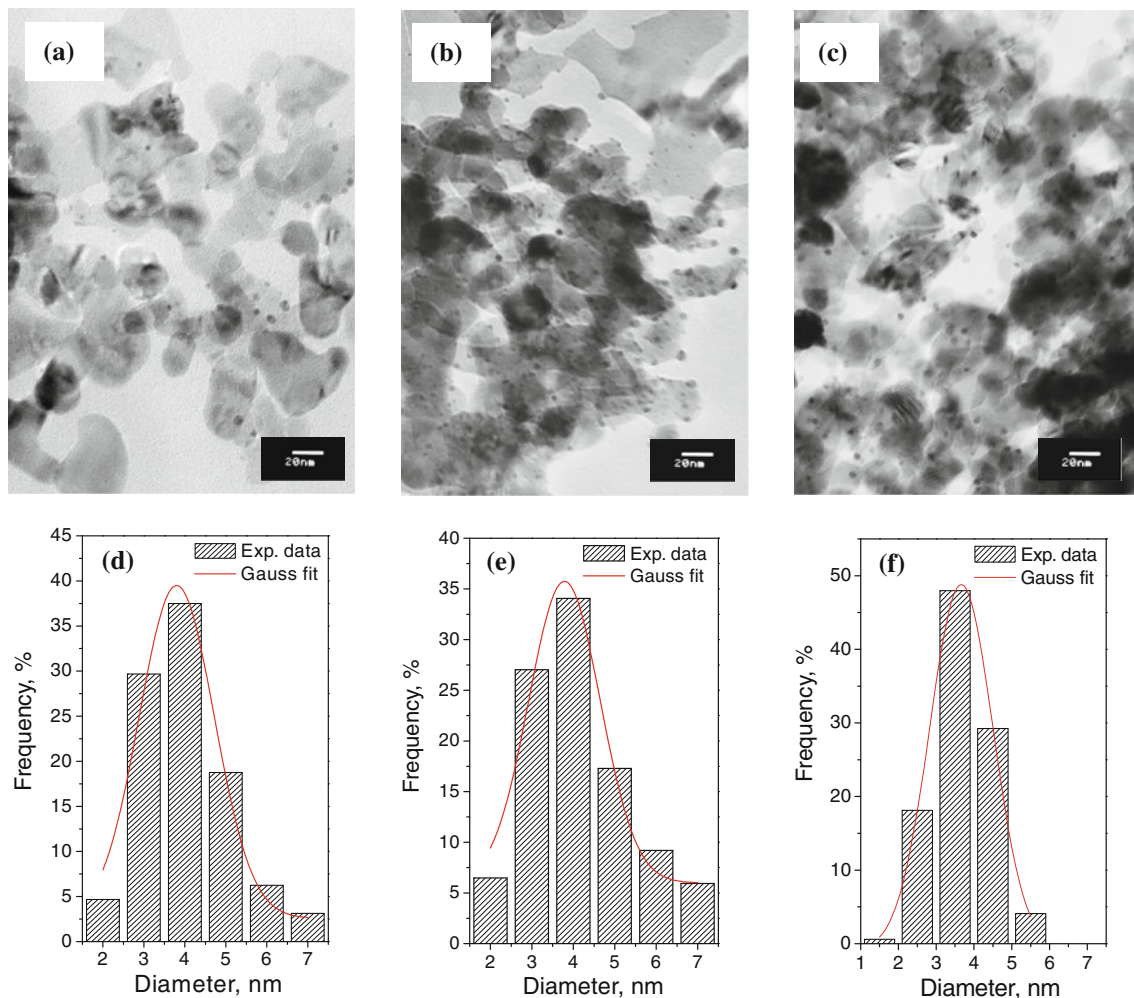


**Fig. 3** Bright-field micrographs of synthesized nanocomposites 0.8-Au/ZnO (a), 2.5-Au/ZnO (b), 9-Au/ZnO (c) (scale bar correspond to 20 nm) and corresponding size distribution histograms of Au-NPs: (d), (e), and (f)

(0.8-Au/ZnO and 9-Au/ZnO) are presented in Fig. 5. The diffraction rings correspond to both the ZnO and the gold phases. SAED pattern in Fig. 5b is complex and composed of rings and spots. The arrangement of spots unambiguously shows a preferred orientation of ZnO particles along the (0001) planes. The SAED data are summarized in Table 3, with interpretation accuracy of 1%. It was established that dominant phases in both samples are the hexagonal ZnO (PDF 89-1397) and Au (PDF 65-2870), but some impurities of cubic phase ZnO (PDF 65-0682) appear. Therefore, the SAED analysis confirms the results obtained from XRD and gives additional information for the presence of trace amounts of cubic ZnO, which could not be detected by XRD.

XPS study of pure ZnO and Au/ZnO nanocomposites was carried out for obtaining some important information about surface compositions and chemical states. The Au 4f and Zn 3p photoelectron spectrum of the sample with highest gold content (9-Au/ZnO) is presented in Fig. 6a

together with the Zn 3p spectrum for pure ZnO. It can be seen that the Au 4f peaks partially overlap with that of Zn 3p. The Au 4f<sub>7/2</sub> peak is clearly observed at binding energy of 83.2 eV, while the Au 4f<sub>5/2</sub> peak is buried in the strong Zn 3p. Figure 6a shows also the reduced Au 4f spectrum after the Zn 3p peak was subtracted from the spectrum. So, in the difference spectrum the Au 4f<sub>7/2</sub> and Au 4f<sub>5/2</sub> peaks are located at 83.2 and 87 eV, with a spin-orbit splitting of 3.7 eV. The BE positions are much lower than that of bulk metallic gold (84.0 and 87.6 eV [35]). However, similar binding energy was reported for supported Au-NPs on  $\gamma$ -Al<sub>2</sub>O<sub>3</sub> [36] and on TiO<sub>2</sub> [37, 38]. One reason for such pronounced negative shift could be the larger electronegativity of gold relative to Zn, leading to a charge transfer from the support to the Au-NPs. Besides, the particle shapes could be a critical factor in determining the negative BE shifts of gold-supported nanoparticles [38]. Radnik et al. [38] found that the more spherical the nanoparticles, the lower the binding energy is (down to

**Fig. 4** HRTEM image of the sample 0.8-Au/ZnO (*left*) and enlargement Fourier filtered area (*right*) (scale bar corresponds to 10 nm)

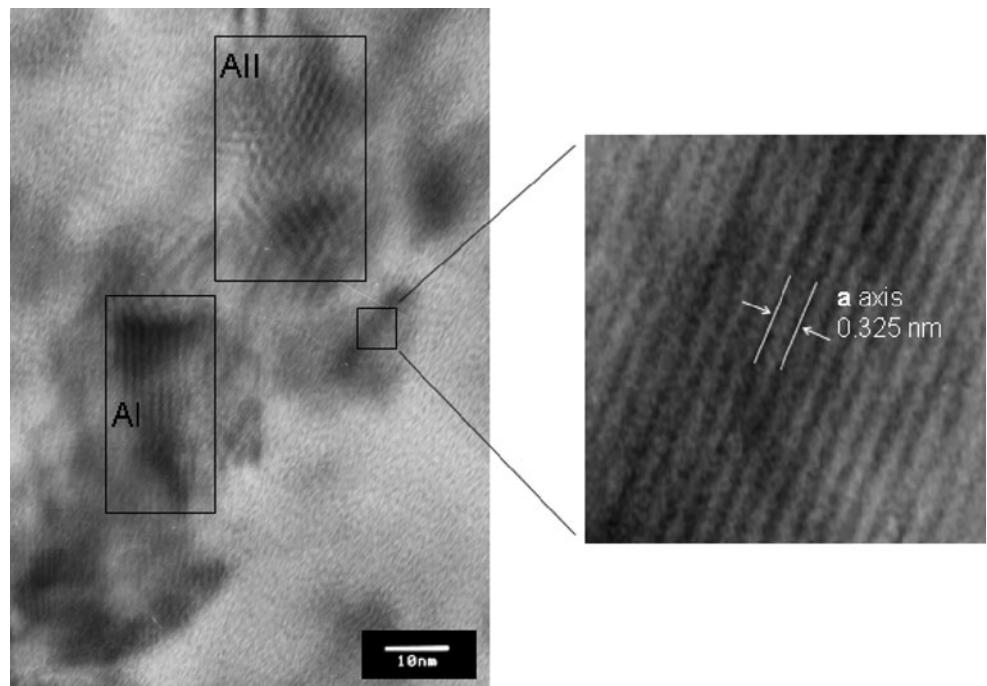
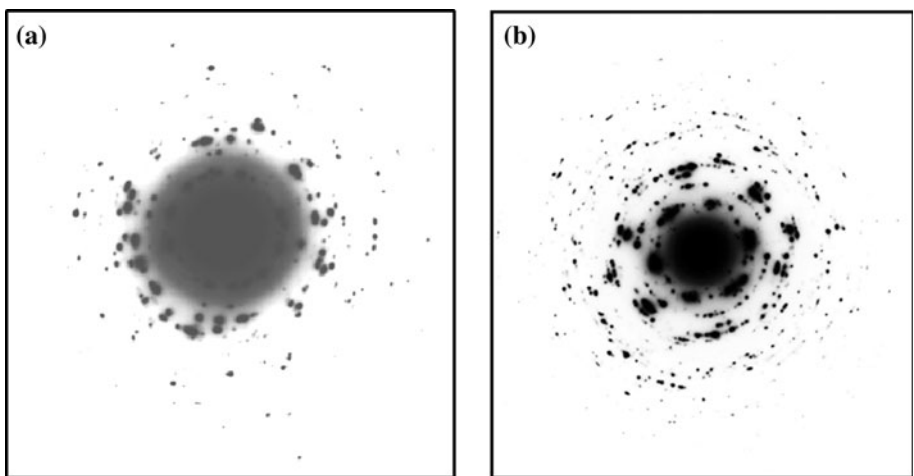


**Fig. 5** Selected area electron diffraction (SAED) patterns of samples with the lowest and the highest gold contents [0.8-Au/ZnO (**a**) and 9-Au/ZnO (**b**)]



83.0 eV for Au on TiO<sub>2</sub>). This shift is attributed to initial state effects, since the spherical particles have less coordinated surface atoms, which reduces their binding energies relative to nanoparticles with large faces. This low coordination of surface Au atoms is the most possible reason for the observed lowering in the binding energy in this study, as the nanoparticle sizes of the 9-Au/ZnO sample are spread between 1 and 6 nm, with the average size of  $3.7 \pm 0.7$  nm.

The O 1s spectra of all studied samples are presented in Fig. 6b. The asymmetric shoulder at a higher binding energy of the O 1s peak is generally ascribed to the adsorbed OH<sup>-</sup> (or H<sub>2</sub>O) species on the surface. The insertion of Au-NPs leads to gradual decrease of the intensity of the oxygen peak.

In order to determine the influence of the gold loading on the chemical environment of zinc, we calculated the modified Auger parameter  $\dot{\alpha}$  for the different samples. It is shown [39] that  $\dot{\alpha}$  ( $\dot{\alpha} = E_K(\text{Zn LMM}) + E_B(\text{Zn } 2p_{3/2})$ ) can be used for more exact determination of the chemical state of Zn, thus eliminating the surface effects of the electrostatic charging. The obtained values (Table 4) show no noticeable changes in the oxidation state of Zn<sup>2+</sup> and its chemical environment with the increase in gold content from 0.8 to 9%.

To estimate the elemental composition on the surface, the Zn 2p, O 1s and Au 4f (when it is detected) peak areas were divided by the corresponding photoionization cross sections. The data are represented in Table 4. The gold is detected on the surface only for samples 2.5-Au/ZnO and

**Table 3** SAED data of the sample 0.8% Au/ZnO and 9% Au/ZnO;  $(hkl)_f$ —double electron diffraction effects; SAED interpretation: accuracy 1%

$d$ (Å)	Relative intensity		ZnO PDF 89-1397 $a = 3.253$ Å, $c = 5.213$ Å SG P6 <sub>3</sub> mc		ZnO PDF 65-0682 $a = 4.270$ Å SG Fm $\bar{3}m$		Au PDF 65-2870 $a = 4.079$ Å SG Fm $\bar{3}m$	
	0.8% Au	9% Au	0.8% Au	9% Au	0.8% Au	9% Au	0.8% Au	9% Au
2.817		vs		100		—		—
2.816	vs		100		—	—	—	—
2.039	vs		—		—	200		
2.038		s				—	200	
1.760	vs	s	(003) <sub>f</sub>	(003) <sub>f</sub>	(211) <sub>f</sub>	(211) <sub>f</sub>	—	—
1.589		s		110		—	—	—
1.493	vs		103		202		—	—
1.408		s		200		(030) <sub>f</sub>	—	—
1.285	m		004		311		(310) <sub>f</sub>	
1.091	vs		203		—		(321) <sub>f</sub>	
1.068	vs		210		400		—	

vs—very strong; s—strong; m—middle

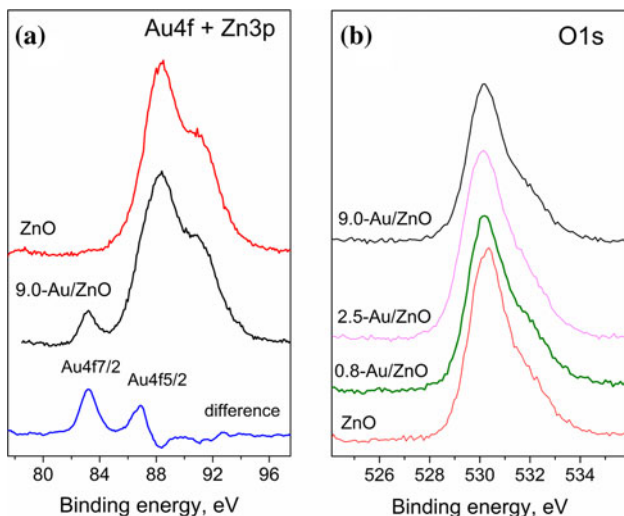


**Fig. 6** Au 4f and Zn 3p photoelectron spectra of pure ZnO and 9-Au/ZnO (a) and the O 1s spectra of all studied samples (b)

9-Au/ZnO which means that its surface content in the 0.8-Au/ZnO is lower than the detection limit of the XPS method. Surprisingly, the surface content of gold obtained

for both samples (2.5-Au/ZnO and 9-Au/ZnO) is quite low and almost the same, despite of the significant difference in their total gold loading. Probably, the segregation of gold species on the crystallite surface of ZnO precursor (basic zinc carbonate) exists as a result of coprecipitation method used, which leads to the interment of significant part of Au-NPs in the volume of ZnO in course of catalyst preparation.

As it can be seen from Table 4, the samples are non-stoichiometric with respect to the Zn/O ratio, which is lower than the value (1.0) for ZnO. With increasing the Au loading, the total surface concentration of oxygen gradually decreased. This is probably due to the fact that the quantity of adsorbed OH<sup>-</sup> groups on the surface of ZnO particles decreases upon the gold loading. Moreover, for sample with highest content of buried Au-NPs (9-Au/ZnO sample), the surface Zn/O ratio is more close to the stoichiometric value, compared to other two samples. It can speculate that the Au-NPs in the bulk ZnO provoke local deformations in the support structure and subsequent migration of interstitial zinc from the volume to the surface of 9-Au/ZnO nanocomposite catalyst.

**Table 4** Surface composition (in atomic percents—At.%) of the studied samples estimated from the XPS data, the Auger parameter values for Zn (in eV), and relative surface content of gold (in %)

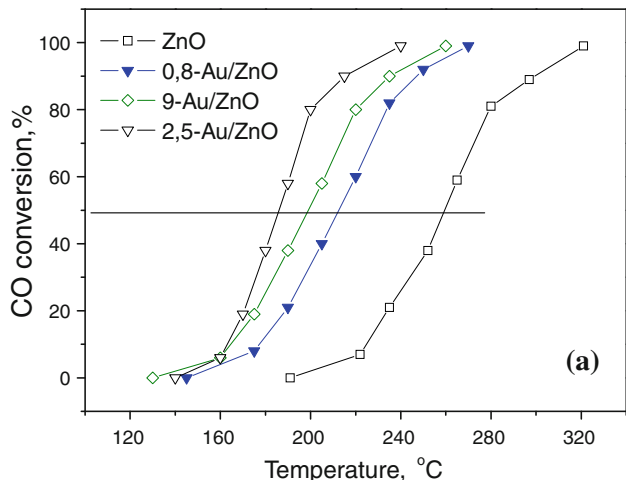
Sample	Content, At.%			Auger parameter, $\alpha$ (eV)	Relative surface Au content <sup>a</sup> , %
	Zn	O	Au		
Pure ZnO	36.6	63.4		2010.5	—
0.8-Au/ZnO	37.4	62.6	Not detected	2010.3	<1.0
2.5-Au/ZnO	37.7	61.9	0.4	2010.4	16.1
9-Au/ZnO	44.8	54.6	0.6	2010.1	6.6

<sup>a</sup> Relative surface Au content is calculate as a ratio of surface Au content to the total Au content

## Catalytic activity

Figure 7a represents the catalytic activity (expressed as a degree of CO conversion- $\eta$ , %) of pure ZnO catalyst and coprecipitated Au/ZnO nanocomposites with different gold loadings (0.8, 2.5, and 9% Au). The results show that the catalytic activity of all Au/ZnO nanocomposites is much higher as compared to pure ZnO. Unexpectedly, the obtained catalytic results show no gradual increase of the catalytic activity with the increase in gold loading from 0.8 to 9% Au. Despite of the 11-fold higher gold content of 9-Au/ZnO as compared to 0.8-Au/ZnO, only a minor increase in the activity is observed. The most active catalyst is 2.5-Au/ZnO nanocomposite. Conversion degree of 93% is reached with this catalyst at 220 °C, while only 7% CO is converted by pure ZnO at this temperature. Another way for estimating the catalytic activity is the comparison of the temperatures for attaining 50% conversion of CO. In the comparison with  $T_{\eta=50\%}$  of pure ZnO, the nanocomposites show a decrease in  $T_{\eta=50\%}$  between 45 and 80 °C depending of the gold loading.

The results of catalytic activity presented as a degree of CO conversion are influenced by the gold loading, the mass of the charged catalysts, and their specific surface area. To estimate separately the effect of gold loading on the effectiveness of catalysts, the temperature dependence of the so called intrinsic activity— $I_s$  (gram of CO converted by 1 m<sup>2</sup> surface of 1 g of catalyst per hour) is found as presented in Fig. 7b. The mutual location of curves remains the same, but their slope decreases to a different extent at the end of the catalytic process, depending on the gold loading. As estimated, the effective purification accomplished by 1 m<sup>2</sup> of catalyst surface is promoted by Au-NPs from 7 (0.8-Au/ZnO) up to 13 times (2.5-Au/ZnO) at 220 °C.



It is important to note that the catalytic activity of the nanocomposites is not affected by the nanoparticle size, since the Au-NPs average diameter for the different samples synthesized is almost the same (~4 nm). Therefore, the results from Fig. 7 manifest the influence of the gold loading level on the catalytic activity. The increase of activity follows the sequence 0.8, 9, and 2.5% Au, i.e., the catalytic activity is not proportional to the gold loading. Hence, an optimal content of the Au nanoparticles corresponding to the best catalytic performance exists for coprecipitated Au/ZnO catalyst. Such optimum has been already reported for Au/MgO and Pd/MgO catalysts obtained by a deposition precipitation method and explained by an increase in the number of dispersed active sites before reaching the aggregation limit of the nanoparticles on the MgO cubes after that the decrease in the catalytic activity is observed [13].

The existence of optimum gold loading in our coprecipitated Au/ZnO catalysts could not be related to the surface state of Au-NPs because their surface amount is a minor fraction of the total gold loading (Table 4). The optimum could not be connected with the surface content of Au-NPs also because the latter increases with the total gold loading, albeit disproportionately. As it can be seen from Table 4, the optimum gold loading for best catalytic performance corresponds to a maximum value of the relative content of Au-NPs on the catalyst surface, calculated as a ratio of surface content to the total content of gold. Therefore, the catalytic activity of coprecipitated Au/ZnO catalysts is noticeably influenced by the distribution of Au-NPs between the bulk and surface of catalysts. It is difficult to distinguish the role of the surface and subsurface Au-NPs on the catalytic performance of the coprecipitated Au/ZnO catalysts, but the effect of buried gold NPs is clearly expressed. According to Nickolov et al. the

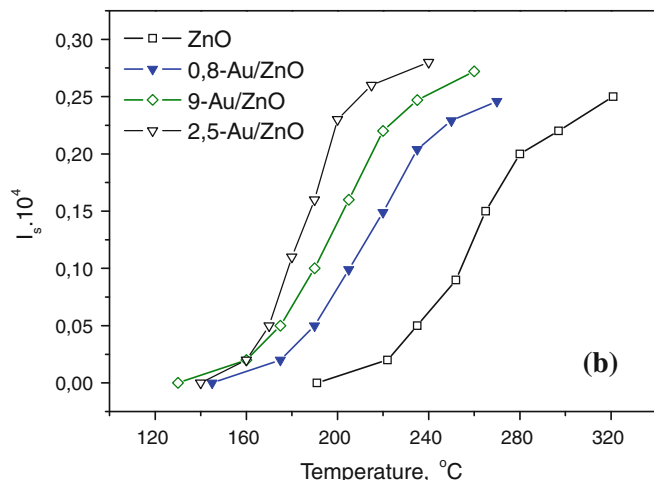


**Fig. 7** Temperature dependence of the degree of CO conversion— $\eta$ , % (a), and intrinsic activity— $I_s$  (gram of CO converted by 1 m<sup>2</sup> surface of 1 g of catalyst per hour) (b)

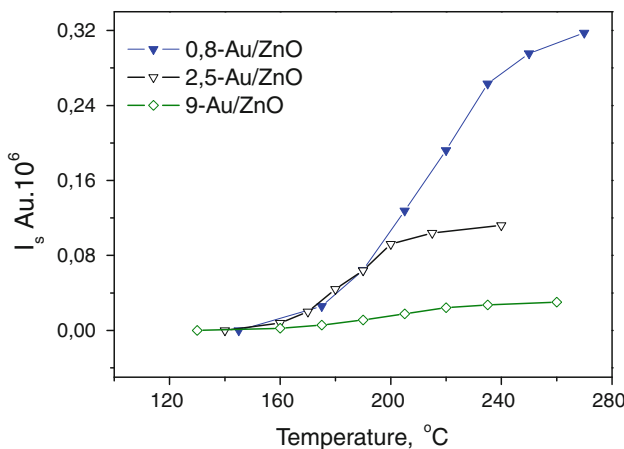


**Fig. 8** Catalytic effectiveness of gold, introduced into the nanocomposite,  $I_s$  Au (intrinsic activity— $I_s$  per 1 g Au) versus temperature

activity of supported heterogeneous catalysts depends to a large extent on the formation of catalytic active complex (CAC) on the support surface. It contains catalytic active sites, which may be separate species of the supported phase in different oxidation states, and surface groups of the support as well, each of them playing a definite role in the catalytic process [40]. The structural data and catalytic test results of our coprecipitated catalysts show that the subsurface Au-NPs affect the stoichiometry of the support, thus changing the activity of CACs probably through the modification of electrostatic interaction between the support and surface Au-NPs. The last suggestion is in accord with conclusions of Phala et al. that the role of ZnO in Au/ZnO catalysts is not merely to disperse gold atoms/particles, but also modify their electronic properties [41].

In order to prepare low cost catalysts containing noble metals, it is important to estimate the catalytic effectiveness of the noble component introduced in the nanocomposite ( $I_s$  Au in our case). The values of  $I_s$  Au are calculated as the intrinsic activity  $I_s$  is normalized to the total gold loading in the nanocomposites. The results are depicted in Fig. 8. In contradistinction from the catalytic activity of nanocomposites (Fig. 7), which passes through a maximum, the catalytic effectiveness of Au-NPs decreases with increasing the gold loading: the lower the total gold loading, the higher the effectiveness of Au is. It can be concluded that the gold in the nanocomposite with the lowest Au content is the most efficient in the catalytic reaction studied, even though this is not the sample that exhibits the highest catalytic activity.

## Conclusions

The Au/ZnO catalysts with gold loading of 0.8, 2.5, and 9% Au are synthesized by a coprecipitation method, and efficiency of gold loading in the range of 86–93% is

achieved. The size of the deposited Au-NPs is not affected by the different gold amounts in the nanocomposites, and an average particle diameter of ca. 4 nm is established from the TEM observation. Spherical shape and homogeneous distribution of Au-NPs in the Au/ZnO nanocomposites are observed in all the samples prepared.

The surface morphology, crystal lattice parameters of ZnO, average crystallite size of the matrix, and chemical environment of  $Zn^{2+}$  are not influenced by incorporation of Au-NPs in the ZnO matrix and do not show noticeable changes upon increasing gold loading from 0.8 to 9%. However, a gradual decrease in the total surface oxygen is observed, probably due to the decrease of adsorbed  $OH^-$  groups upon gold loading. The migration of interstitial zinc from the volume to the surface of support is established, influenced by the high amount of Au-NPs buried in ZnO matrix at gold loading of 9%.

The Au-NPs considerably promote the catalytic activity of zinc oxide for CO oxidation. The conversion degree of 93% is reached with the most active catalyst at 220 °C, while only 7% CO is converted by pure ZnO at this temperature. At the same Au-NP size, the decrease of catalytic activity of the nanocomposites follows the sequence 2.5, 9, and 0.8% Au, so an optimal total loading of the Au nanoparticles exists for the best performance of coprecipitated Au/ZnO catalyst. This optimum corresponds to the optimal distribution of Au-NPs between surface and volume of the support, which ensures both maximum relative surface content of Au-NPs and high nonstoichiometry of the support.

**Acknowledgements** This study has been financially supported by the Scientific Research Fund of Sofia University, Bulgaria (Project 014/2010). The authors are thankful to Dr. Peter Tzvetkov (Bulgarian Academy of Sciences) for interpretation of the XRD data.

## References

1. Haruta M, Sano H, Kobayashi T (1987) US Patent 4698324
2. Haruta M, Kobayashi T, Sano H, Yamada M (1987) Chem Lett 16:405–408
3. Hutchings GJ (1985) J Catal 96:292
4. Haruta M, Hutchings GJ (2005) Appl Catal A Gen 291:2
5. Haruta M (1997) Catal Today 36:153
6. Choudhary TV, Goodman DW (2002) Top Catal 21:25
7. Bond GC, Thompson DT (1999) Catal Rev Sci Eng 41:319
8. Chen MS, Goodman DW (2006) Catal Today 111:22
9. Cuena BR (2010) Thin Solid Films 518:3127
10. Bond GC, Louis C, Thompson DT (2006) In: Catalysis by gold. Imperial College Press, London
11. Grisel R, Weststrate KJ, Gluhoi A, Nieuwenhuys BE (2002) Gold Bull 35:39
12. Bamwenda GR, Tsubota S, Nakamura T, Haruta M (1997) Catal Lett 44:83
13. Glaspell G, Hassan HMA, Elzatahy A, Fuoco L, Radwan NRE, El-Shall MS (2006) J Phys Chem B 110:21387

14. Carabineiro SAC, Machado BF, Bacsa RR, Serp P, Dražić G, Faria JL, Figueiredo JL (2010) *J Catal* 273:191
15. Bocuzzi F, Chiorino A, Tsubota S, Haruta M (1994) *Catal Lett* 29:225
16. Hutchings GJ, Siddiqui MRH, Burrows A, Kiely CJ, Whyman R (1997) *J Chem Soc Faraday Trans* 93:187
17. Wang GY, Zhang WX, Lian HL, Jiang DZ, Wu TH (2003) *Appl Catal A Gen* 239:1
18. Al-Sayari S, Carley AF, Taylor SH, Hutchings GJ (2007) *Top Catal* 44:123
19. Souza KR, de Lima AFF, de Sousa FF, Appel LG (2008) *Appl Catal A Gen* 340:440
20. Naknam P, Luengnaruemitchai A, Wongkasemjit S (2009) *Energy Fuels* 23:5084
21. Naknam P, Luengnaruemitchai A, Wongkasemjit S (2009) *Int J Hydr Energy* 34:9838
22. Tabakova T, Idakiev V, Andreeva D, Mitov I (2000) *Appl Catal A Gen* 202:91
23. Wu JJ, Tseng CH (2006) *Appl Catal B Environ* 66:51
24. Li C, Li L, Du Z, Yu H, Xiang Y, Li Y, Cai Y, Wang T (2008) *Nanotechnology* 19:035501 (4 pp)
25. Hongsith N, Viriyaworasakul C, Mangkorntong P, Mangkorntong N, Choopun S (2008) *Ceram Int* 34:823
26. Wongrat E, Pimpang P, Choopun S (2009) *Appl Surf Sci* 256:968
27. Bocuzzi F, Chiorino A, Tsubota S, Haruta M (1995) *Sens Actuators B Chem* 25:540
28. Chang SJ, Hsueh TJ, Chen IC, Huang BR (2008) *Nanotechnology* 19:175502 (5 pp)
29. Joshi RK, Hu Q, Alvi F, Joshi N, Kumar A (2009) *J Phys Chem C* 113:16199
30. Wongchoosuk C, Choopun S, Tuantranont A, Kerdcharoen T (2009) *Mater Res Innov* 13:185
31. Haruta M, Sano H (1984) *Shokubai (Catalyst)* 26:140
32. Hao Z, Fen L, Lu GQ, Liu J, An L, Wang H (2001) *Appl Catal A Gen* 213:173
33. Kraus V, Nolze J (2000) Powder cell, version 2.4
34. Chen CC, Liu P, Lu CH (2008) *Chem Eng J* 144:509
35. Moulder TF, Stickle WF, Sobol PE, Bomben KD (1992) *Handbook of X-ray photoelectron spectroscopy*. Perkin-Elmer, Eden Prairie
36. Veith GM, Lupini AR, Pennycook SJ, Ownby GW, Dudney NJ (2005) *J Catal* 231:151
37. Do Y, Choi JS, Kim SK, Sohn Y (2010) *Bull Korean Chem Soc* 31:2170
38. Radnik J, Mohr C, Claus P (2003) *Phys Chem Chem Phys* 5:172
39. Futsuhara M, Yoshioka K, Takai O (1998) *Thin Solid Films* 322:274
40. Nickolov R, Tsonecheva T, Mehandjiev D (2002) *Fuel* 81:203
41. Phala NS, Klatt G, van Steen E, French SA, Sokol AA, Catlow CRA (2005) *Phys Chem Chem Phys* 7:2440